

# Linear Attention for Joint Power Optimization and User-Centric Clustering in Cell-Free Networks

Irched Chafaa, Giacomo Bacci, Senior Member, IEEE, Luca Sanguinetti, Fellow, IEEE

Abstract—Optimal access point (AP) clustering and power allocation are essential in user-centric cell-free massive MIMO systems. However, existing solutions, whether based on deep learning or traditional optimization, lack flexibility to adapt to dynamic network configurations, neglect pilot contamination effects and incur significant computational complexity. In this paper, we propose a lightweight Transformer model that overcomes these limitations by jointly predicting AP clusters and powers solely from the knowledge of spatial coordinates of user devices and APs. Our model is architecture-agnostic to users load, handles both clustering and power allocation without channel estimation overhead, and eliminates pilot contamination by assigning users to APs within a pilot reuse constraint. We also incorporate a customized linear attention mechanism to capture user-AP interactions efficiently and enable linear scalability with respect to the number of users. Numerical results confirm the model’s effectiveness in maximizing the minimum spectral efficiency and providing near-optimal performance while ensuring adaptability and scalability in dynamic scenarios.

Index Terms—CosFormer, Transformer, linear attention, supervised learning, power optimization, user-centric cell-free massive MIMO.

## I. Introduction

Cell-free (CF) massive MIMO (mMIMO) has emerged as a promising architecture to overcome the limitations of conventional cellular networks [1]–[4]. Unlike traditional cellular systems, where each user equipment (UE) is associated with a single base station, CF mMIMO deploys a large number of distributed access points (APs) that coherently and jointly serve all UEs within the coverage area. This high level of cooperation offers uniform service quality, mitigates inter-cell interference, and enhances spectral efficiency (SE), particularly in dense or heterogeneous environments. However, realizing these benefits in practice remains challenging. If every AP serves every UE, the resulting system demands substantial fronthaul

signaling, creates unnecessary interference from weak AP-UE links, and leads to inefficient use of power and pilot resources [5].

To address these challenges, the user-centric (UC) paradigm has been introduced in CF mMIMO [6]–[9]. In this approach, each UE is served by a subset of the most relevant APs, selected based on spatial proximity or channel quality. By restricting cooperation to the most beneficial APs, the UC strategy reduces interference and enhances scalability by lowering the computational and signaling burden. Nevertheless, the performance of UC CF mMIMO depends critically on the proper selection of AP clusters and transmission powers, which must adapt dynamically to variations in channel conditions, UE mobility, and network configurations. This makes clustering and power control crucial challenges in realizing the full potential of UC CF mMIMO.

## A. Related work

Given the importance of clustering and power optimization in UC CF mMIMO, a wide range of solutions have been proposed in the literature [6], [10]–[18]. These approaches differ in whether they treat clustering and power allocation separately or jointly, and in the methodologies employed, ranging from classical optimization to modern machine learning.

Classical optimization-based methods have long been applied to power allocation, often through iterative algorithms [6], [10] or closed-form solutions for specific objectives such as the max-min fairness (MMF) problem [11]. While these approaches can achieve near-optimal performance, they typically require multiple iterations to converge, resulting in high computational complexity and poor scalability in dynamic networks.

In parallel, clustering strategies have been studied extensively. Heuristic approaches [12], [13] provide simple rules for grouping users and APs, while optimization-based formulations [14] aim for more principled solutions. More recently, deep learning models [15] have been introduced to automate clustering decisions. Despite their advantages, these methods often lack adaptability: heuristic rules may oversimplify, optimization approaches remain computationally demanding, and deep learning solutions require retraining whenever the number of UEs or APs changes.

Joint clustering and power allocation has also been investigated [16]–[18], with the goal of simultaneously determining the serving AP subset and transmission

The authors are with the Dipartimento di Ingegneria dell’Informazione, University of Pisa, Via Caruso 16, 56122, Pisa, Italy (e-mail: irched.chafaa@ing.unipi.it, {giacomo.bacci, luca.sanguinetti}@unipi.it). This work was supported by the Smart Networks and Services Joint Undertaking (SNS JU) under the European Union’s Horizon Europe research and innovation program under Grant Agreement No 101192369 (6G-MIRAI), and by the project FoReLab (Departments of Excellence), funded by the Italian Ministry of Education and Research (MUR). L. Sanguinetti was also supported by the Project GARDEN funded by EU in NextGenerationEU Plan through Italian “Bando Prin 2022-D.D.1409 del 14-09-2022”.

powers. These methods generally outperform separate treatments, but they still suffer from scalability issues and often neglect critical aspects such as pilot contamination. Overall, whether treated separately or jointly, existing solutions remain limited in their ability to adapt efficiently to dynamic network conditions.

### B. Transformer-based power allocation

Recently, Transformers [19] have been explored to address flexibility in dynamic wireless networks. In [20], the authors propose a Transformer-based model only for down-link (DL) power allocation to handle varying numbers of UEs via unsupervised learning. However, the proposed method requires post-processing and padding, which introduces excessive padding when UE loads vary widely, potentially diluting meaningful information, and increases computational load without contributing useful information [21], [22], thereby slowing training and affecting convergence. In [23], we addressed the flexibility issue in CF mMIMO by leveraging a Transformer-based model capable of handling varying user densities without padding or retraining. Unlike [20], which employs large-scale fading coefficients as input, our model uses only spatial information (AP/UE coordinates) to jointly predict up-link (UL) and DL powers. This design enables efficient adaptation to changes in the number of UEs and APs, while maintaining near-optimal performance for the MMF problem. Nevertheless, the solution did not address AP clustering or pilot contamination, and its complexity still scaled quadratically with the number of users similarly to [20]. In summary, the key question motivating this work is: How can we overcome these limitations while preserving the advantages of Transformer-based models in dynamic CF mMIMO?

### C. Main contributions

Building on our earlier work in [23], this paper develops a scalable geometry-driven optimization framework for UC CF mMIMO systems. The proposed model learns to approximate channel-aware max-min SE optimization policies while significantly reducing computational and signaling overhead.

The main contributions are summarized as follows:

- Scalable joint clustering and power control: We propose a single end-to-end learning framework that jointly predicts AP clusters and UL/DL power under a max-min fairness objective. Unlike prior methods that rely on repeated channel information for resource allocation, the proposed approach produces near-optimal decisions using only spatial coordinates as input, reducing overhead and decoupling clustering and power control from channel estimation and data detection. Since UE positions capture key propagation and interference characteristics, the model learns this mapping while naturally adapting to varying UE loads.
- Linear-complexity attention for large-scale CF networks: The proposed model employs a customized linear attention mechanism whose complexity scales linearly with the number of UEs. This makes the framework suitable for dense UC deployments where quadratic-attention Transformers or optimization methods become computationally prohibitive. In addition, the exponential linear unit (ELU)-based mapping improves numerical conditioning and helps preserving weaker but fairness-relevant AP-UE interactions in large heterogeneous networks.
- Adaptation to varying UE loads without architectural redesign: The architecture is permutation-invariant and operates with different numbers of UEs without architecture modification or retraining, addressing a key limitation of existing deep learning-based resource allocation schemes.
- Pilot-aware architectural constraint: A pilot-related clustering constraint is embedded directly within the encoder, ensuring that each AP serves no more UEs than the available orthogonal pilots. This mitigates pilot contamination effects without requiring additional pilot assignment procedures.
- Robustness to imperfect spatial information: We explicitly evaluate robustness to coordinate estimation errors by injecting Gaussian perturbations into UE positions during training and testing. The results demonstrate stable performance under input uncertainty, enhancing practical deployment feasibility.

### D. Paper outline and notation

The remainder of the paper is organized as follows. Sects. II and III describe the wireless network model and the problem formulation. Sect. IV introduces the proposed ELU-CosFormer architecture for AP clustering and power optimization, while Sect. V details the training procedure. Sect. VI presents an extensive performance evaluation, and Sect. VII provides a computational complexity analysis. Conclusions and potential future extensions are discussed in Sect. VIII.

We denote the sets of real and complex numbers by  $\mathbb{R}$  and  $\mathbb{C}$ . Matrices and vectors are written in boldface upper- and lowercase letters, respectively. The superscripts  $(\cdot)^T$  and  $(\cdot)^H$  denote the transpose and the conjugate transpose operations, respectively, and  $\odot$  indicates element-wise multiplication. Element indices are written as  $a_i$  for the  $i$ th entry of vector  $\mathbf{a}$  and  $a_{i,j}$  for the  $(i, j)$ th entry of a matrix. The notation  $\mathcal{N}_C(\boldsymbol{\mu}, \mathbf{C})$  refers to a circularly symmetric complex Gaussian variable with mean  $\boldsymbol{\mu}$  and covariance matrix  $\mathbf{C}$ . The norm  $\|\cdot\|$  denotes the  $\ell_2$  vector norm, and  $\mathbb{E}[\cdot]$  the expectation operator. The notation  $\mathbb{1}(\cdot)$  refers to the indicator function. The  $N \times N$  identity matrix and the all-zero vector with  $N$  elements are denoted by  $\mathbf{I}_N$  and  $\mathbf{0}_N$ , respectively.

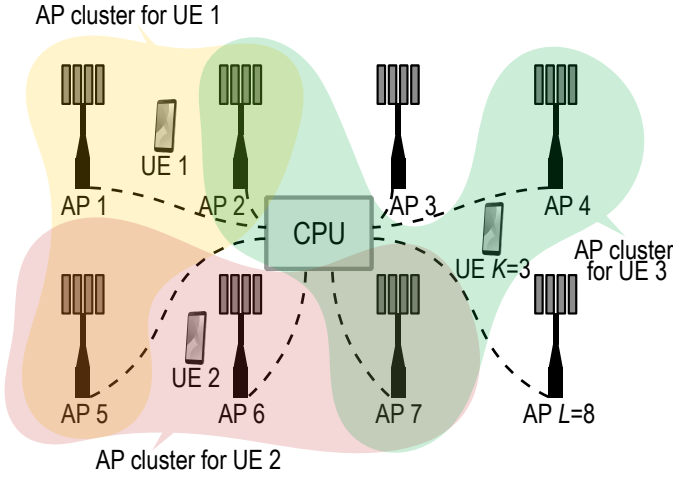


Fig. 1: Illustration of a UC CF mMIMO network, with  $L = 8$  APs and  $K = 3$  UEs. Each UE is served by its own cluster of APs.

## II. Wireless Network Model

We consider a UC CF mMIMO network, like the one shown in Fig. 1, with  $K$  single-antenna UEs and  $L$  APs, each having  $N$  antennas (in this example, we use  $K = 3$ ,  $L = 8$ , and  $N = 4$ ). Each UE is served by a subset of APs, called cluster and indicated by the different colors in Fig. 1, and each AP can serve at most  $\tau_p$  UEs to prevent pilot contamination. The network operates under a standard time division duplexing (TDD) protocol [6], where the  $\tau_c$  symbols of each coherence block are allocated to UL training ( $\tau_p$ ), UL data ( $\tau_u$ ), and DL data ( $\tau_d$ ), with  $\tau_c \geq \tau_p + \tau_u + \tau_d$ . We adopt a narrowband channel model and assume that channels remain constant over a coherence block. The channel vector between AP  $l$  and UE  $k$  is denoted by  $\mathbf{h}_{lk}$  and modeled as [6]:

$$\mathbf{h}_{lk} = \sqrt{\beta_{lk}} \mathbf{R}_{lk}^{1/2} \mathbf{g}_{lk}, \quad (1)$$

where  $\beta_{lk}$  is the large-scale fading, accounting for path loss and shadowing,  $\mathbf{R}_{lk} \in \mathbb{C}^{N \times N}$  is the spatial correlation matrix at AP  $l$ , and  $\mathbf{g}_{lk} \sim \mathcal{N}_C(\mathbf{0}, \mathbf{I}_N)$  is an i.i.d. complex Gaussian vector representing the small-scale fading, where  $\mathbf{I}_N$  is the  $N \times N$  identity matrix. We assume that the channels  $\{\mathbf{h}_{lk}; l = 1, \dots, L\}$  are independent and call  $\mathbf{h}_k = [\mathbf{h}_{1k}^T, \dots, \mathbf{h}_{Lk}^T]^T \in \mathbb{C}^{LN}$  the collective channel from all APs to UE  $k$ .

The central processing unit (CPU), also shown in Fig. 1, computes the estimate of  $\mathbf{h}_k$  on the basis of received pilot sequences transmitted during the training phase [6]. The minimum mean square error (MMSE) estimate is  $\hat{\mathbf{h}}_k = [\hat{\mathbf{h}}_{1k}^T, \dots, \hat{\mathbf{h}}_{Lk}^T]^T$  with [6, Sect. IV]

$$\hat{\mathbf{h}}_{lk} = \mathbf{R}_{lk} \mathbf{Q}_{lk}^{-1} \left( \mathbf{h}_{lk} + \frac{1}{\tau_p \rho} \mathbf{n}_{lk} \right) \sim \mathcal{N}_C(\mathbf{0}_N, \Phi_{lk}), \quad (2)$$

where  $\rho$  is the UL pilot power of each UE,  $\mathbf{n}_{lk} \sim \mathcal{N}_C(\mathbf{0}_N, \sigma^2 \mathbf{I}_N)$  is the thermal noise, and  $\Phi_{lk} =$

$\mathbf{R}_{lk} \mathbf{Q}_{lk}^{-1} \mathbf{R}_{lk}$ , where  $\mathbf{Q}_{lk} = \mathbf{R}_{lk} + \frac{\sigma^2}{\tau_p \rho} \mathbf{I}_N$ . Hence,  $\hat{\mathbf{h}}_k \sim \mathcal{N}_C(\mathbf{0}_{LN}, \Phi_k)$ , with  $\Phi_k = \text{diag}(\Phi_{1k}, \dots, \Phi_{Lk})$ . Note that the method proposed in this paper can be applied to other channel estimation schemes.

### A. Uplink and downlink spectral efficiency

An achievable UL SE of UE  $k$  is given by the use-and-then-forget bound [6, Sect. V]:

$$\text{SE}_k^{\text{UL}} = \frac{\tau_u}{\tau_c} \log_2 \left( 1 + \text{SINR}_k^{\text{UL}} \right), \quad (3)$$

with UE  $k$ 's effective signal-to-interference-plus-noise ratio (SINR) defined as

$$\frac{p_k^{\text{UL}} |\mathbb{E}\{\mathbf{v}_k^H \mathbf{D}_k \mathbf{h}_k\}|^2}{\sum_{i=1}^K p_i^{\text{UL}} \mathbb{E}\{|\mathbf{v}_k^H \mathbf{D}_k \mathbf{h}_i|^2\} - p_k^{\text{UL}} |\mathbb{E}\{\mathbf{v}_k^H \mathbf{D}_k \mathbf{h}_k\}|^2 + \sigma^2 \mathbb{E}\{\|\mathbf{D}_k \mathbf{v}_k\|^2\}}. \quad (4)$$

Here,  $p_k^{\text{UL}}$  is the UL transmit power of user  $k$ ,  $\mathbf{v}_k \in \mathbb{C}^N$  is the combining vector, and  $\mathbf{D}_k = \text{diag}(\mathbf{D}_{k1}, \dots, \mathbf{D}_{kL})$  is a block-diagonal matrix with  $\mathbf{D}_{kl} = \mathbf{I}_N$  if AP  $l$  serves UE  $k$ , and  $\text{diag}(\mathbf{0}_N)$  otherwise. The expectation is taken with respect to all sources of randomness. Although the bound in (3) is valid for any combiner  $\mathbf{v}_k$ , we consider the MMSE, given by [6, Sect. V]:

$$\mathbf{v}_k = \left( \sum_{k=1}^K p_k^{\text{UL}} \hat{\mathbf{h}}_k \hat{\mathbf{h}}_k^H + \mathbf{Z} \right)^{-1} \hat{\mathbf{h}}_k, \quad (5)$$

where

$$\mathbf{Z} = \sum_{k=1}^K p_k^{\text{UL}} [\text{diag}(\mathbf{R}_{1k}, \dots, \mathbf{R}_{Lk}) - \Phi_k] + \sigma^2 \mathbf{I}_{LN}. \quad (6)$$

Similarly, the DL SE of user  $k$  is [6, Sect. VI]

$$\text{SE}_k^{\text{DL}} = \frac{\tau_d}{\tau_c} \log_2 \left( 1 + \text{SINR}_k^{\text{DL}} \right), \quad (7)$$

where UE  $k$ 's effective SINR is

$$\frac{p_k^{\text{DL}} |\mathbb{E}\{\mathbf{h}_k^H \mathbf{D}_k \mathbf{w}_k\}|^2}{\sum_{i=1}^K p_i^{\text{DL}} \mathbb{E}\{|\mathbf{h}_k^H \mathbf{D}_i \mathbf{w}_i|^2\} - p_k^{\text{DL}} |\mathbb{E}\{\mathbf{h}_k^H \mathbf{D}_k \mathbf{w}_k\}|^2 + \sigma^2}. \quad (8)$$

Here,  $p_k^{\text{DL}}$  is the total DL power allocated to serve UE  $k$  such that  $p_k^{\text{DL}} = \sum_{l=1}^L p_{k,l}^{\text{DL}}$ , with  $p_{k,l}^{\text{DL}} \in [0, \bar{P}_l^{\text{DL}}]$  being AP  $l$ 's transmit power allocated for user  $k$ ;  $\bar{P}_l^{\text{DL}}$  is the maximum power per AP (when user  $k$  is not served by AP  $l$ ,  $p_{k,l}^{\text{DL}} = 0$ ); and  $\mathbf{w}_k \in \mathbb{C}^{LN}$  is the associated unit-norm precoding vector. The MMSE precoder is used [6], which is given by  $\mathbf{w}_k = \mathbf{v}_k / \|\mathbf{v}_k\|$ . The channel estimation and precoding/combining models adopted above are used to generate channel-aware training data as explained later in Sect. V-A. The proposed learning framework itself does not require instantaneous channel information at the CPU during inference, as it predicts clustering and power decisions directly from UE/ AP spatial information, although channel variations are implicitly embedded during training (see Sect. V-B for further details).

### III. Problem Formulation

To ensure fairness among UEs, we adopt the MMF problem, widely used in UC CF mMIMO systems [6], [11], [24]. In the UL, the problem takes the form [6, Sect. VII]:

$$\begin{aligned} & \max_{\{p_k^{\text{UL}} \geq 0\}} \min_k \text{SE}_k^{\text{UL}} \\ & \text{subject to } p_k^{\text{UL}} \leq \bar{P}_k^{\text{UL}} \quad \forall k \end{aligned} \quad (9)$$

where  $\bar{P}_k^{\text{UL}}$  is the maximum UL power for UE  $k$ . Similarly, in the DL we have that:

$$\begin{aligned} & \max_{\{p_{k,l}^{\text{DL}} \geq 0\}} \min_k \text{SE}_k^{\text{DL}} \\ & \text{subject to } \sum_{k=1}^K p_{k,l}^{\text{DL}} \leq \bar{P}_l^{\text{DL}} \quad \forall l. \end{aligned} \quad (10)$$

The optimization problems in (9) and (10) can be solved using a closed-form solution [11], iterative solvers (e.g., [6], [10]), or deep learning models (e.g., [20], [25], [26]) following these common steps:

- 1) Estimate the large-scale fading coefficients;
- 2) Assign serving AP clusters to the UEs using a clustering algorithm (e.g., the dynamic cooperation clustering (DCC) scheme in [9]);
- 3) Estimate the channel vectors  $\mathbf{h}_{l,k}$  between APs and UEs;
- 4) Compute the combining and precoding vectors ( $\mathbf{v}_k$  and  $\mathbf{w}_k$ );
- 5) Evaluate the SE using (3) or (7);
- 6) Compute the UL and DL transmit powers by solving (9) and (10).

Irrespective of the adopted methodology, the solution must be obtained in real time, i.e., fast enough to be deployed before the UEs' positions, load, and spatial distribution change and the clustering and power allocation problems need to be solved again. This stringent latency requirement limits the flexibility of the system with respect to varying UE loads and results in impractical computational overhead in large and dynamic networks, since a new solution must be computed at every coherence block. In particular, the closed-form solution in [11] provides the optimal solution to (9) and (10) for a given fixed clustering configuration. However, it does not address the joint clustering and power allocation problem, and its computational complexity scales cubically with the number of UEs.

To address these limitations, we propose a learning model based on CosFormer [27]. We show that the geographical locations of UEs and APs provide sufficient information to serve as a proxy for jointly determining the clusters and computing the optimal power allocation. We advocate using the UEs' positions since they capture the key characteristics of propagation channels and interference patterns in the network. The proposed model

learns this mapping while naturally handling varying UE loads. Once trained, the model bypasses the repeated execution of the full optimization pipeline (i.e., the six steps listed above) and produces near-optimal decisions through a single forward pass, enabling scalable and real-time adaptation to varying UE loads while preserving fairness.

Furthermore, this framework enables a separation between resource allocation – potentially performed at the CPU – and data detection, carried out at the APs, thereby further improving system scalability. Finally, the proposed approach can also serve as an effective system design tool, as it relies only on coarse information (i.e., the UE locations).

#### A. Overview of CosFormer

The standard Transformer [19] relies on an attention mechanism that captures dependencies among tokens (UEs in our case), but its quadratic complexity limits scalability. CosFormer [27] overcomes this issue by introducing a linearized attention mechanism that preserves accuracy while significantly reducing computational cost. Among linear Transformer variants [28]–[30], CosFormer is particularly well suited to our setting due to the following properties:

- 1) Accurate and stable attention: While many linear variants approximate the softmax attention and thus incur approximation errors, CosFormer replaces softmax with a cosine-based reweighting, improving numerical stability and avoiding such errors.
- 2) Implicit spatial bias: The cosine reweighting naturally emphasizes local relationships, which aligns with the importance of nearby AP-UE pairs for clustering and power allocation.
- 3) Computational efficiency: CosFormer attains linear complexity, reducing memory use and accelerating training, an essential feature for scalability in large CF networks.

Building on this foundation, we introduce our modified architecture, ELU-CosFormer, which augments CosFormer [27] with pilot-aware constraints and modified activation functions. These enhancements enable the model to jointly predict AP clusters and powers while eliminating pilot contamination and ensuring SE fairness. Once trained with data that include channel modeling and estimation, ELU-CosFormer produces clusters and UL/DL power levels directly from the spatial positions of the UEs and APs, allowing seamless adaptation to varying user loads.

#### IV. Proposed Learning Model for Clustering and Power Optimization

In this section, we introduce the proposed learning model, ELU-CosFormer, which performs joint AP clustering and UL/DL power allocation. We first describe the overall model architecture, and subsequently detail

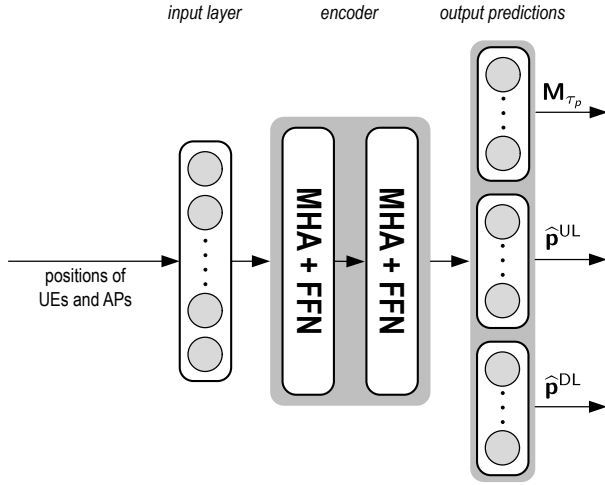


Fig. 2: Architecture diagram of the proposed model to predict jointly AP clusters, UL and DL powers leveraging spatial information at the input.

the linearized attention mechanism based on the modified CosFormer formulation.

#### A. Model architecture

The proposed model is a CosFormer-based neural network composed of three main components: a dynamic input layer, a stack of encoder layers, and parallel output heads for clustering and power prediction (see Fig. 2). These three components are described next in detail.

- 1) Input layer: The input tensor is  $\mathbf{X} \in \mathbb{R}^{K \times (2L+2)}$ , where each UE is represented by  $2L + 2$  spatial features (coordinates of all  $L$  APs and the UE itself). This tensor is projected into an embedding space of dimension  $d_{\text{mod}}$  via a linear layer:

$$\mathbf{Z}_{\text{in}} = \mathbf{X}\mathbf{W}_{\text{in}}^{\top} + \mathbf{b}_{\text{in}}, \quad (11)$$

with trainable parameters  $\mathbf{W}_{\text{in}}$  and  $\mathbf{b}_{\text{in}}$ . The input is a sequence of  $K$  tokens, where each token corresponds to one UE. Since the same projection is applied independently to every token, the operation does not assume a fixed number of UEs. Consequently, changes in  $K$  only modify the sequence length, while the model parameters remain unchanged. The subsequent encoder processes this sequence using shared weights among UEs and preserves the sequence token-structure, enabling the learning model to handle varying user loads seamlessly without requiring architectural modifications.

- 2) Encoder layers: The embedded tensor  $\mathbf{Z}^{(0)} = \mathbf{Z}_{\text{in}} \in \mathbb{R}^{K \times d_{\text{mod}}}$  is processed through  $M$  encoder layers. Each layer consists of a modified CosFormer multi-head attention (MHA), denoted by  $\mathcal{A}(\cdot)$ , followed by a feed-forward network (FFN). Moreover, the encoder layers apply layer normalization and residual connections to stabilize training and preserve information across

layers [27]. Specifically, the  $m$ -th encoder layer applies the following operations (see Fig. 3):

$$\mathbf{Z}_1^{(m)} = \mathbf{Z}^{(m-1)} + \mathcal{A}(\tilde{\mathbf{Z}}^{(m-1)}), \quad (12)$$

$$\mathbf{H}^{(m)} = \text{ReLU}(\tilde{\mathbf{Z}}_1^{(m)} \mathbf{W}_1^{(m)\top} + \mathbf{b}_1^{(m)}), \quad (13)$$

$$\mathbf{Z}^{(m)} = \tilde{\mathbf{Z}}_1^{(m)} + \mathbf{H}^{(m)} \mathbf{W}_2^{(m)\top} + \mathbf{b}_2^{(m)}, \quad (14)$$

where  $\tilde{\mathbf{Z}}$  denotes a layer-normalized version of a tensor  $\mathbf{Z}$ ;  $\mathbf{W}_1^{(m)}$ ,  $\mathbf{b}_1^{(m)}$ ,  $\mathbf{W}_2^{(m)}$ , and  $\mathbf{b}_2^{(m)}$  are trainable parameters; ReLU refers to an activation function [31] introducing a non-linearity.

All  $M$  layers share the same structure, and the output of each encoder layer preserves the dimension  $\mathbb{R}^{K \times d_{\text{mod}}}$ , serving as input to the next layer. After  $M$  layers, the final tensor  $\mathbf{Z}^{(M)} = \mathbf{Z}_{\text{out}}$  represents the encoder output that will be processed next by the output heads. The attention mechanism in (12)-(14) is detailed in Sect. IV-B.

- 3) Output heads: Three parallel heads operate on the final encoder output  $\mathbf{Z}_{\text{out}} \in \mathbb{R}^{K \times d_{\text{mod}}}$ :

- UC clustering mask: A fully-connected layer with sigmoid activation [31] produces an initial mask tensor  $\mathbf{M} \in \mathbb{R}^{K \times L}$ , where each entry represents the association strength between a UE and an AP:

$$\mathbf{M} = \text{sigmoid}(\mathbf{Z}_{\text{out}} \mathbf{W}_{\text{mask}} + \mathbf{b}_{\text{mask}}), \quad (15)$$

with trainable parameters  $\mathbf{W}_{\text{mask}}$  and  $\mathbf{b}_{\text{mask}}$ .

To mitigate pilot contamination, a two-step procedure is applied. First, for each AP, only the top  $\tau_p$  UEs with the highest mask scores are retained via  $\text{Top}_{\tau_p}(\mathbf{M})$ . Then, a thresholding operation assigns the AP to serve the UE if the retained score exceeds a threshold  $\xi$ , yielding the final binary clustering mask:

$$\mathbf{M}_{\tau_p} = \mathbb{1}(\text{Top}_{\tau_p}(\mathbf{M}) \odot \mathbf{M} > \xi). \quad (16)$$

The threshold  $\xi$  is a hyperparameter tuned during training to balance connectivity and interference. Proper selection of  $\xi$  ensures strong UE-AP associations while maintaining high SE.

- Uplink power prediction: A fully-connected layer with sigmoid activation predicts normalized UL powers:

$$\tilde{p}_k^{\text{UL}} = (\text{sigmoid}(\mathbf{Z}_{\text{out}} \mathbf{W}_{\text{UL}} + \mathbf{b}_{\text{UL}}))_k, \quad (17)$$

where  $\mathbf{W}_{\text{UL}}$  and  $\mathbf{b}_{\text{UL}}$  are trainable parameters. The denormalized UL powers are obtained as

$$\hat{p}_k^{\text{UL}} = \Delta_{\text{UL}} \tilde{p}_k^{\text{UL}} + \underline{P}_{\text{UL}}, \quad (18)$$

where  $\Delta_{\text{UL}} = \overline{P}_{\text{UL}} - \underline{P}_{\text{UL}}$  denotes the UL power range. Here,  $\overline{P}_{\text{UL}}$  and  $\underline{P}_{\text{UL}}$  are the maximum and minimum allowable UL transmit powers.

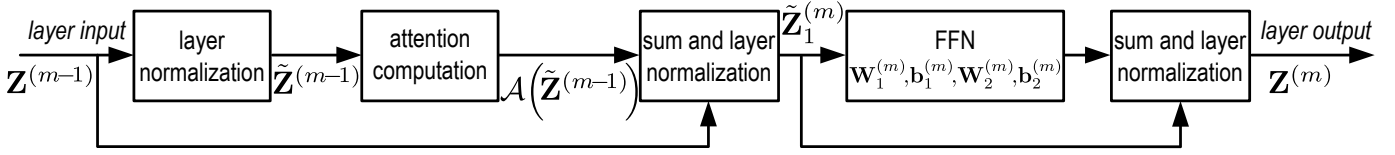


Fig. 3: Illustration diagram of operations in one encoder layer.

- Downlink power prediction: A fully-connected layer with sigmoid activation outputs normalized per-AP DL power weights:

$$\tilde{p}_{k,l}^{\text{DL}} = (\text{sigmoid}(\mathbf{Z}_{\text{out}} \mathbf{W}_{\text{DL}} + \mathbf{b}_{\text{DL}}))_{k,l}, \quad (19)$$

where  $\mathbf{W}_{\text{DL}}$  and  $\mathbf{b}_{\text{DL}}$  are trainable parameters, and  $\tilde{p}_{k,l}^{\text{DL}} \in [0, 1]$  represents the relative power weight assigned by AP  $l$  to UE  $k$ .

To enforce the per-AP power constraint in (10), the predicted weights are scaled by the AP power budget:

$$\hat{p}_{k,l}^{\text{DL}} = \frac{\tilde{p}_{k,l}^{\text{DL}}}{\sum_{i=1}^K \tilde{p}_{i,l}^{\text{DL}}} \bar{P}_l^{\text{DL}}. \quad (20)$$

Since the available DL power labels are defined per UE, the total predicted DL power allocated to UE  $k$  is computed as  $\hat{p}_k^{\text{DL}} = \sum_{l=1}^L \hat{p}_{k,l}^{\text{DL}}$ . These values are then normalized using the min-max scaling criterion introduced in Sect. V-A (Step 3) to obtain the predicted labels used for training. This ensures that the learning model respects the per-AP power constraints while remaining consistent with the available optimal labels used in the loss function defined in Sect. V-B.

## B. Attention mechanism

We now detail the attention mechanism used in (12)-(14). The queries ( $\mathbf{Q}$ ), keys ( $\mathbf{K}$ ), and values ( $\mathbf{V}$ ) [19] are simultaneously computed from the layer-normalized input  $\tilde{\mathbf{Z}}_{\text{in}}$  using a single linear transformation:

$$\mathbf{\Omega} = \tilde{\mathbf{Z}}_{\text{in}} \mathbf{W}_{\Omega} + \mathbf{b}_{\Omega}, \quad (21)$$

where  $\mathbf{W}_{\Omega} \in \mathbb{R}^{d_{\text{mod}} \times 3d_{\text{mod}}}$  and  $\mathbf{b}_{\Omega} \in \mathbb{R}^{3d_{\text{mod}}}$  are trainable parameters. The resulting tensor  $\mathbf{\Omega} \in \mathbb{R}^{B \times K \times 3d_{\text{mod}}}$  is split along the last dimension into three parts, yielding  $\mathbf{Q}, \mathbf{K}, \mathbf{V} \in \mathbb{R}^{B \times K \times d_{\text{mod}}}$ . These are then reshaped into  $N_h$  attention heads of dimension  $d_{\text{head}} = d_{\text{mod}}/N_h$ , giving

$$\mathbf{Q}, \mathbf{K}, \mathbf{V} \in \mathbb{R}^{B \times N_h \times K \times d_{\text{head}}}. \quad (22)$$

A kernel feature mapping  $\phi(\cdot)$  is applied to the queries and keys:

$$\mathbf{Q}' = \phi(\mathbf{Q}), \quad (23)$$

$$\mathbf{K}' = \phi(\mathbf{K}), \quad (24)$$

with  $\phi(\cdot)$  being an activation function chosen to approximate the softmax kernel [31] of the original Transformer while enabling linearized attention.

The attention is then computed via a linearized operation:

$$\mathbf{A} = \mathbf{Q}' \cdot \left( (\mathbf{K}'^{\top} \cdot \mathbf{V}) \cdot \mathbf{W} \right), \quad (25)$$

where  $\mathbf{W} \in \mathbb{R}^{K \times K}$  is a fixed cosine reweighting matrix with entries  $w_{ij} = \cos(\pi(i-j)/(2K))$ . This modulation biases attention toward nearby tokens, mimicking the locality bias of softmax without computing full pairwise interactions, thereby avoiding the quadratic complexity. In our context, this allows the model to distinguish between nearby and distant UEs/APs without introducing additional trainable parameters.

Finally,  $\mathbf{A}$  is projected back into the model dimension, yielding the final attention weights used in (12):

$$\mathbf{A}(\tilde{\mathbf{Z}}^{(m-1)}) = \mathbf{A} \mathbf{W}_{\text{out}}^{\top} + \mathbf{b}_{\text{out}}, \quad (26)$$

with  $\mathbf{W}_{\text{out}} \in \mathbb{R}^{d_{\text{mod}} \times d_{\text{mod}}}$  and  $\mathbf{b}_{\text{out}} \in \mathbb{R}^{d_{\text{mod}}}$  being trainable parameters.

Our choice of activation function. In the original CosFormer [27], the kernel feature mapping function  $\phi(\cdot)$  is implemented using rectified linear unit (ReLU). In this work, we propose a simple yet efficient modification: replacing ReLU with the ELU [31]. This choice is motivated by both physical insights and empirical evidence. Formally, the two activations are defined as [31]:

$$\text{ReLU}(x) = \max(0, x),$$

$$\text{ELU}(x) = \begin{cases} x & \text{if } x > 0, \\ \alpha(e^x - 1) & \text{if } x \leq 0, \end{cases} \quad (27)$$

where  $\alpha$  is a hyperparameter, typically set to 1.

ELU provides smoother gradients and nonzero outputs for negative inputs, preserving richer feature interactions and improving gradient flow and numerical stability during training. This is particularly important in our setting, where spatial coordinates require the attention mechanism to capture subtle UE-AP variations. In contrast, ReLU zeroes out all negative inputs, potentially discarding useful spatial information and leading to sparse gradients that hinder convergence. By deliberately allowing negative values, ELU maintains continuity across the input domain and prevents inactive attention heads, enabling the attention mechanism to exploit weak but meaningful AP-UE associations that would otherwise be suppressed. Such associations are critical under MMF criterion, where low-gain links can influence the performance of the worst-case UE.

Moreover, the exponential tail of ELU produces a smooth and fully differentiable activation, which interacts naturally with the cosine modulation in (25) (through  $\mathbf{W}$ ). This combination yields a differentiable kernel that results in smoother and more stable attention distributions, reducing abrupt variations in the attention weights. This behavior is consistent with the inherently smooth spatial variations observed in wireless propagation, where signal strengths change gradually rather than abruptly. Consequently, the learned attention patterns better reflect realistic relationships between UEs and APs, leading to more physically meaningful clustering boundaries and a more balanced power allocation across the network. The effectiveness of this activation function is evaluated in Sect. VI via an ablation experiment.

## V. Training Setup

The model is trained offline to predict the AP clusters and UE powers. Next, we explain the structure of the generated dataset and provide details about the training process.

### A. Dataset Construction

To train and evaluate the learning model, we construct, based on the model in Sect. II, a synthetic dataset that captures diverse cell-free network configurations and realistic deployment conditions. The dataset construction follows four main steps:

Step 1) Data generation: For each configuration defined by a pair  $(K, L)$ , we generate:

- random 2D positions within a bounded area for  $K$  single-antenna UEs, denoted as  $\{\mathbf{u}_k\}_{k=1}^K$ , with  $\mathbf{u}_k \in \mathbb{R}^2$ , and  $L$  uniformly distributed APs, denoted as  $\{\mathbf{a}_l\}_{l=1}^L$ , with  $\mathbf{a}_l \in \mathbb{R}^2$ ;
- large-scale fading coefficients  $\beta_{lk}$ , correlation matrices  $\mathbf{R}_{lk}$ , MMSE estimated channels  $\hat{\mathbf{h}}_{lk}$ , MMSE precoders  $\mathbf{w}_k$  and combiners  $\mathbf{v}_k$  computed as detailed in Sect. II, which are required later by the closed-form solution to solve the max-min SE optimization problems in (9) and (10) for each set of clusters.

Step 2) Noise injection: To simulate localization errors and improve robustness, Gaussian noise is added to UE positions:

$$\mathbf{u}'_k = \mathbf{u}_k + \delta_k, \quad \delta_k \sim \mathcal{N}(0, \sigma_e^2), \quad (28)$$

where  $\sigma_e = 1$  m, following [32]. This perturbation accounts for position estimation errors.

Step 3) Normalization: All features are normalized to the range  $[0, 1]$  using min-max scaling. For a feature vector  $\boldsymbol{\xi}$ , we use

$$\tilde{\boldsymbol{\xi}} = \frac{\boldsymbol{\xi} - \min(\boldsymbol{\xi})}{\max(\boldsymbol{\xi}) - \min(\boldsymbol{\xi}) + \varepsilon}, \quad (29)$$

where  $\varepsilon$  is a small constant to avoid division by zero. Coordinates are normalized separately for  $x$

---

## Algorithm 1 Training with Dynamic Supervision

---

Require: Training dataset  $\{\mathbf{X}_i\}_{i=1}^S$ , batch size  $S$ , trade-off parameter  $\lambda$

- 1: for each epoch do
- 2:   for each batch do
- 3:     Compute attention scores from the input  $\mathbf{X}_i$
- 4:     Generate AP clusters for each UE
- 5:     Compute powers by solving (9) and (10) [11]
- 6:     Evaluate the loss function (30)
- 7:     Update model parameters via backpropagation
- 8:   end for
- 9: end for

---

and  $y$ , preserving geometric relationships, while UL and DL powers are normalized globally to ensure consistent scaling.

Step 4) Dataset overview: A total of 8000 training samples are generated for each value of  $K \in \{5, 10\}$  and  $L = 16$ . Each sample consists of normalized noisy UE and AP coordinates, with corresponding optimal powers computed on the fly during training. To evaluate generalization, additional samples are generated for other user counts beyond the training values of  $K$ , enabling assessment of the model's ability to adapt to unseen network configurations. Overall, the dataset includes diverse configurations by varying the number of UEs, their spatial distributions, and channel realizations, ensuring robust learning and effective generalization.

### B. Training approach

Unlike conventional supervised learning [33], the optimal power labels cannot be precomputed prior to training because the clusters of APs serving each UE are determined dynamically by the model itself. Consequently, the optimal power labels depend on the clustering decisions produced during the forward pass and are computed on-the-fly during training. This results in a supervised learning framework with dynamic label generation, also referred to as dynamic supervision [34], [35], where the supervision signals are obtained by solving the power control problems for the clusters predicted by the model.

The overall training procedure is summarized in Algorithm 1. During the forward pass, the model evaluates attention scores between the input features, which define the AP clusters by assigning a set of serving APs to each UE. Given these predicted clusters, the UL and DL power control problems are solved using the closed-form expressions in [11]. Then, the predicted powers  $\tilde{\mathbf{p}}$  are compared with the normalized optimal ones  $\tilde{\mathbf{p}}^*$ , and the loss function updates the model parameters:

$$\mathcal{L} = \frac{1}{S} \sum_{i=1}^S \|\tilde{\mathbf{p}}_i^* - \tilde{\mathbf{p}}_i\|^2 - \lambda \left( \min_k \text{SE}_k^{\text{UL}} + \min_k \text{SE}_k^{\text{DL}} \right), \quad (30)$$

Table I: Model architecture parameters.

Parameter	Value
Encoder layers $M$	2
Attention heads $N_h$	4
Model dimension $d_{\text{mod}}$	64
Clustering threshold $\xi$	0.3

Table II: Model training hyperparameters.

Parameter	Value
Trade-off parameter $\lambda$	$10^{-2}$
Dropout rate	0.1
Optimizer	AdamW [37]
Learning rate	$10^{-3}$
Epochs	20
Batch size	64

where  $S$  is the batch size. The loss combines the mean-squared error between predicted and optimal powers with a clustering-aware penalty that promotes fairness across users. The hyperparameter  $\lambda$  controls the trade-off between minimizing prediction error and improving the worst-case SE. In practice,  $\lambda$  is tuned empirically via cross-validation.

The model is implemented in PyTorch [36] and configured with the parameters listed in Tables I and II, which are empirically tuned to balance accuracy and computational efficiency.

Notably, the model does not take channel coefficients as input; instead, their effect is captured through the optimal power labels. By learning from these labels, the network maps UE-AP spatial configurations to clustering and power allocation decisions across different network configurations and user loads, effectively approximating the max-min SE policy at inference time without requiring instantaneous channel information.

## VI. Numerical results

In this section, we assess the performance of the proposed learning-based framework for solving the MMF problem in the UC CF mMIMO system described in Sect. II. The main simulation parameters are reported in Table III. All numerical results are averaged over the test set.

The proposed solution is compared against the following clustering and power allocation schemes:

- Optimal CF: A fully cooperative baseline in which all APs serve all UEs, and transmit powers are obtained via the closed-form expression in [11].
- DCC: A fixed-clustering benchmark based on the DCC scheme [9], where each UE is associated with its  $Q = 8$  strongest APs. Power control follows the closed-form solution.
- Optimal UC-CF: A hybrid strategy in which AP-UE clusters are inferred by the proposed model, while transmit powers are still computed using the closed-form solution.

Table III: CF mMIMO network parameters.

Parameter	Value
Network area	500 m $\times$ 500 m
Number of APs ( $L$ )	16 (uniformly deployed)
Antennas per AP ( $N$ )	4
Carrier frequency	2 GHz
Path-loss exponent	3.67
UE-AP height difference	10 m
Shadow fading $F_{kl}$	$\mathcal{N}_C(0, \alpha^2)$ , $\alpha^2 = 4$ dB
Noise power $\sigma^2$	-94 dB
Noise figure $\eta$	7 dB
Bandwidth $B$	20 MHz
Max UL transmit power $\bar{P}_{\text{UL}}$	100 mW
Max DL transmit power per AP $\bar{P}_i^{\text{DL}}$	200 mW
Coherence block length $\tau_c$	200
Pilot length $\tau_p$	10
UL data symbols $\tau_u$	90
DL data symbols $\tau_d$	100

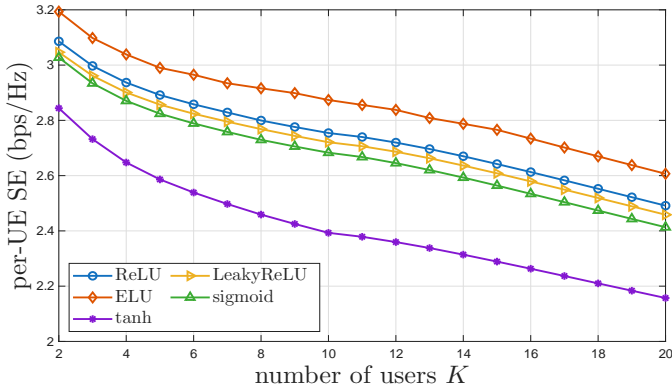
- Predicted UC-CF: The fully data-driven approach, where both clustering decisions and power levels are directly predicted by the proposed learning architecture.

### A. Activation function performance

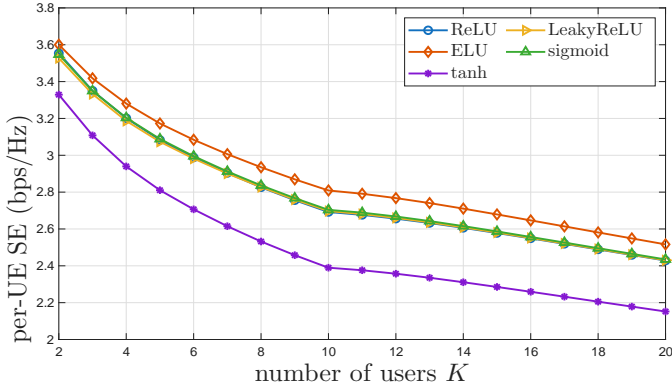
To validate the choice of the ELU activation function detailed in Sect. IV-B, we evaluate the per-UE SE achieved by a CosFormer using several activation functions [31] for the attention computation with the simulation parameters in Table III. The results reported in Fig. 4 demonstrate that ELU consistently yields higher SE across all user counts  $K$  for both UL and DL scenarios, confirming that ELU provides a more effective attention computation for our problem.

### B. Spectral efficiency evaluation

Fig. 5 reports the average per-UE SE as a function of the number of users  $K$  for both UL and DL transmission. As expected, the per-UE SE decreases with increasing  $K$  in both links, since a larger number of users must share a fixed amount of AP resources and is subject to higher interference. Nevertheless, the rate at which performance degrades varies significantly across the considered strategies. In the UL (Fig. 5a), Optimal CF provides the highest SE for small values of  $K$  due to full AP cooperation. However, its performance deteriorates more rapidly as  $K$  increases. Beyond  $K \approx 10$ , Optimal UC-CF surpasses the fully cooperative baseline, as limiting cooperation to the most relevant APs reduces interference and enables a more effective allocation of transmit power. A similar behavior is observed in the DL (Fig. 5b): while full CF remains superior at low user densities, Optimal UC-CF achieves higher SE for larger  $K$ , with the benefits of clustering being even more pronounced in DL due to improved power concentration and reduced inter-user interference. The Predicted UC-CF closely tracks the optimal UC-CF in both UL and DL, confirming the generalization capability of the trained model across unseen user loads. In contrast, the classical DCC consistently yields the lowest SE, as



(a) UL



(b) DL

Fig. 4: Comparison of per-UE SE using different activation functions in CosFormer for UL and DL. ELU yields the highest SE across all UE counts.

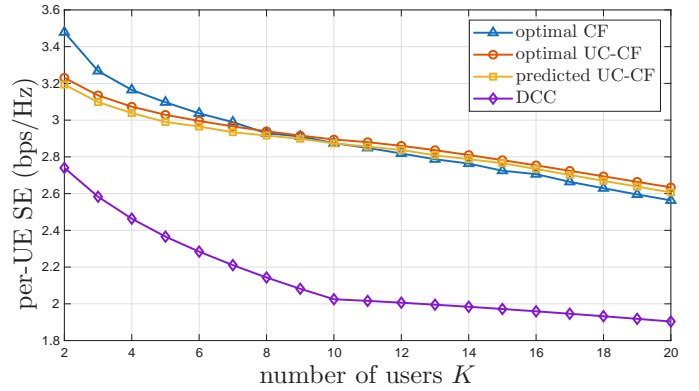
its fixed clustering cannot adapt to varying interference conditions.

Overall, these results show that while fully CF operation is advantageous at low UE densities, UC clustering becomes increasingly beneficial as the network grows congested. The proposed learning model adapts to this transition, sustaining near-optimal performance with reduced computational and signaling overhead.

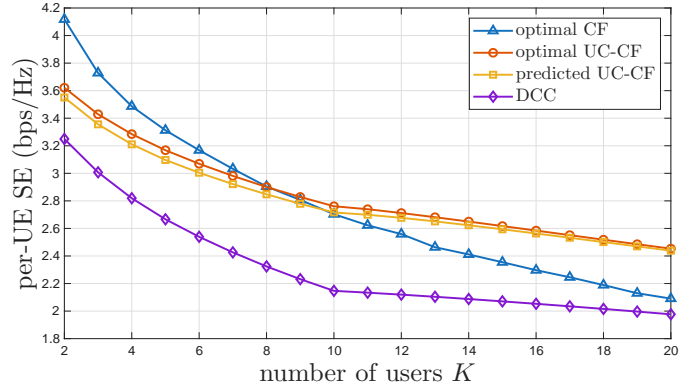
### C. AP-UE clustering performance

In Fig. 6, we evaluate the total number of UE/AP connections (when UE is served by AP) of optimal CF, predicted UC-CF and DCC schemes for different user loads. In addition, we plot, in the secondary Y-axis, the average number of connections per UE of the predicted UC-CF.

The results show that the UC-CF scheme exhibits fewer total connections compared to CF, reflecting the selective association of users to a subset of APs based on the learned clustering. This indicates an efficient usage of network resources since less connections implies less signaling and power consumption while still providing near-optimal SE as illustrated earlier in Fig. 5. Moreover, it can be seen that the total AP-UE connections saturates for higher



(a) UL



(b) DL

Fig. 5: Average per-UE SE in UL and DL for different  $K$  values on the test set. The proposed model adapts better to increasing user load compared to benchmark policies.

user loads as the APs reach their  $\tau_p$ -served UE constraint unlike other policies that keep increasing, affecting their scalability. Correspondingly, the average number of APs per UE (red curve) gradually decreases as  $K$  increases. This behavior confirms the model's ability to dynamically reconfigure clusters and allocate AP efficiently under varying user densities to achieve better scalability. In contrast, the DCC, which always connects the UE to  $Q = 8$  APs, yields the low total connections at first, but at the expense of a poor SE performance (Fig. 5) and a linear growth of AP-UE connections with  $K$ .

Fig. 7 represents an example of the clustering behavior of the model for  $K = 20$  and  $L = 16$  for a given sample of the testing set. Each UE is annotated with the number of APs it is connected to, revealing the model's adaptive clustering. Dashed lines highlight the AP-UE links, showing selective association to only the most relevant APs. This visualization confirms that UC-CF forms compact, user-specific clusters that vary across users, enabling efficient resource allocation and reduced signaling overhead.

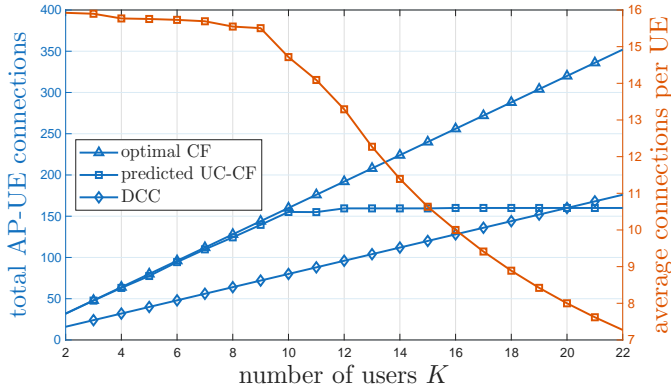


Fig. 6: Total AP-UE connections (left axis) and average connections per UE (right axis) as functions of different user loads. Our model in UC-CF strategy adapts the clusters dynamically to handle the increasing user load.

#### D. Power prediction accuracy

To further evaluate the effectiveness of the proposed learning model, we compare the cumulative distribution functions (CDFs) of UL and DL powers obtained from the optimal closed-form solution [11] and those predicted by the trained model on the test set. As shown in Fig. 8, the resulting curves are nearly overlapping in both cases, indicating that the model successfully learns the underlying power allocation strategy for the predicted clusters. This close agreement demonstrates that the predicted powers not only approximate the optimal allocation with high fidelity but also preserve the statistical distribution of transmit powers across UEs. Consequently, the proposed approach achieves reliable power prediction while avoiding the computational burden of solving the closed-form optimization problem. This behavior is explained by the fact that the optimal power allocation is a mapping of large-scale channel statistics which highly depend on UE-AP geometry, and thus the trained model learns to approximate this mapping accurately even for unseen UE deployments of the test set.

#### E. Robustness to input errors

In Fig. 9, we analyze the robustness of the proposed learning model against input uncertainty. During training, as stated in (28), the model is exposed to user position inputs corrupted by random Gaussian noise with a standard deviation of 1 m. To assess generalization and robustness, the model is evaluated under three test conditions: i) input with a fixed standard deviation error of 3 m, ii) input with a fixed standard deviation error of 5 m, and iii) an ideal scenario with error-free input.

The results show that the per-UE SE decreases only slightly as the input error level increases, for both UL and DL. Specifically, the maximum gap between the error-free and 5 m error cases is approximately 0.29 b/s/Hz in UL and 0.24 b/s/Hz in DL across all user counts,

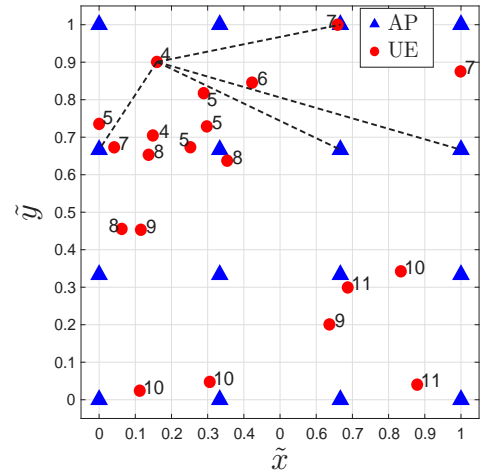
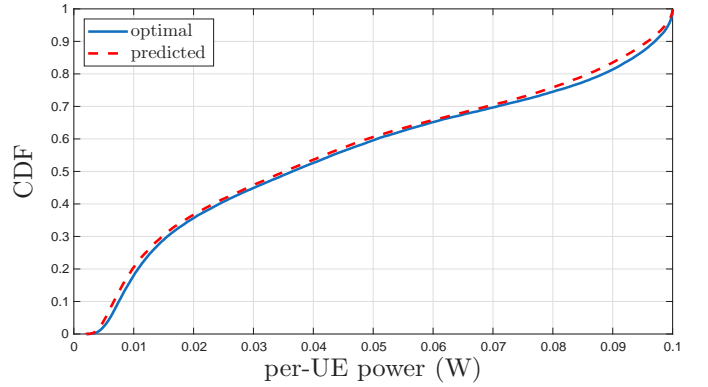
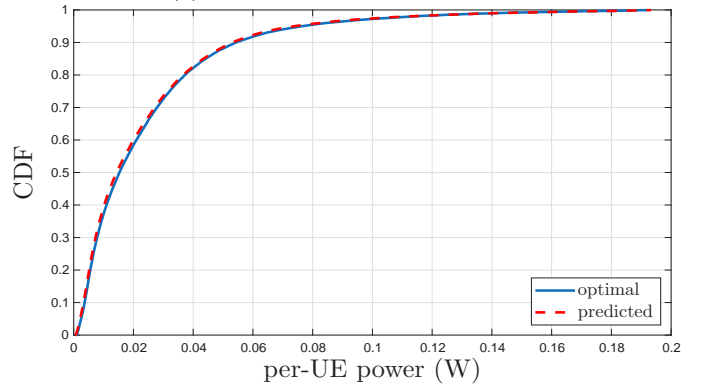


Fig. 7: Network layout of APs and UEs for  $K = 20$  users. User-specific clusters are predicted by the model for efficient resource allocation.



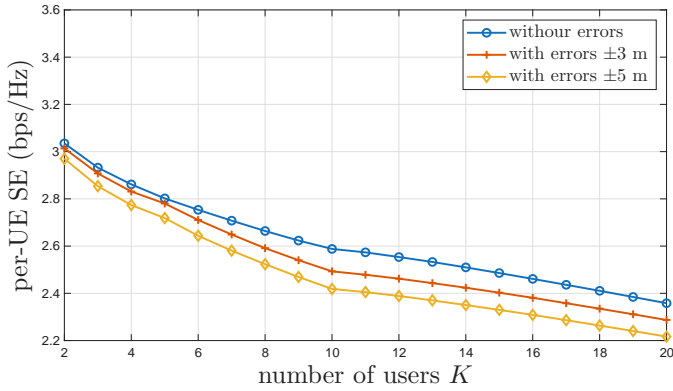
(a) CDF of UL transmit powers.



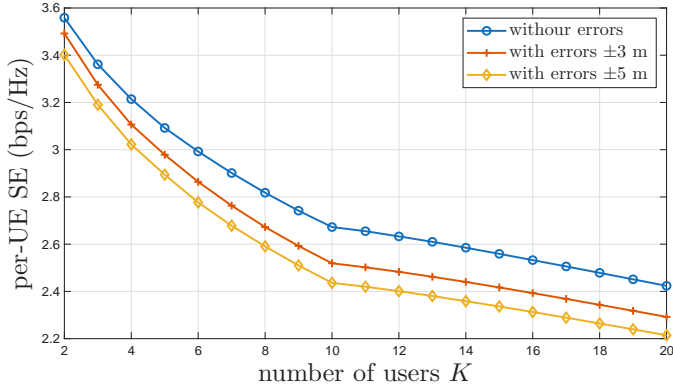
(b) CDF of DL transmit powers.

Fig. 8: CDF comparison of optimal and predicted powers in UL and DL. The close overlap confirms the accuracy of the proposed learning model in reproducing the optimal power statistics.

demonstrating the resilience of the proposed model. Moreover, the relative trends across different user loads are preserved, indicating that the model can generalize its



(a) UL



(b) DL

Fig. 9: Average per-UE SE for different UE counts and input error levels. The trained model remains robust to input errors.

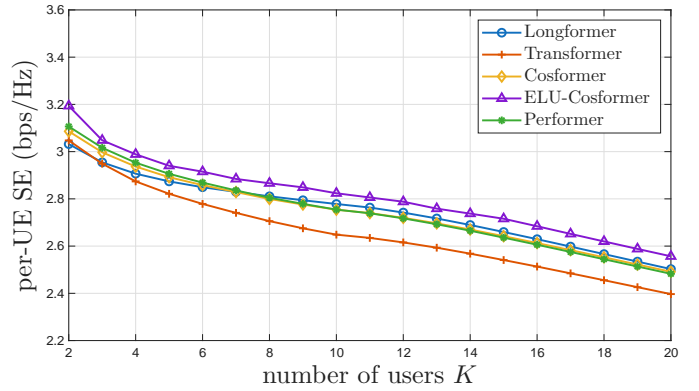
learned spatial relationships even when the inputs are affected by localization errors, thus ensuring practical robustness for real-world deployments where user position estimates are inherently imperfect.

#### F. Comparison with other Transformer variants

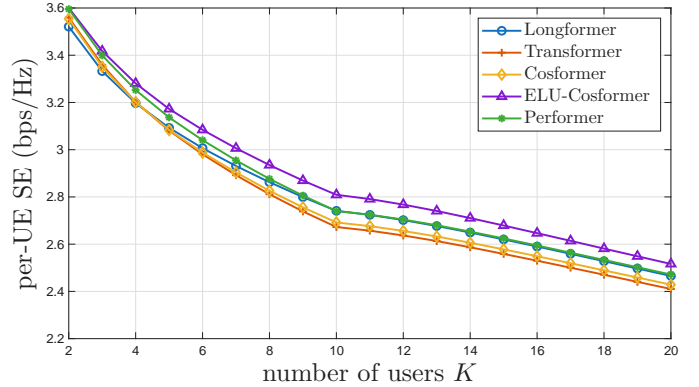
Fig. 10 presents a comparative analysis of UL and DL per-UE SE achieved by the Transformer and four linear attention variants. Linformer is excluded because it cannot accommodate variable UE counts without additional preprocessing or architectural modifications [29].

In both UL and DL scenarios, ELU-CosFormer consistently achieves the highest SE across all user counts. This result highlights the benefit of integrating the ELU activation into the CosFormer attention kernel. As discussed in Sect. IV, the combination of ELU with the cosine-based attention mechanism improves the model's ability to capture the spatial interactions between UEs and APs. Consequently, ELU-CosFormer produces more effective AP clustering and power allocation decisions, maintaining strong performance even as the number of users increases under the considered fairness-driven objective.

In addition to SE, Table IV compares the models in terms of complexity and efficiency metrics. All models



(a) UL



(b) DL

Fig. 10: Comparison of per-UE SE across different Transformer variants for UL and DL scenarios. Our modified CosFormer maintains higher SE.

were evaluated under consistent conditions to ensure fair comparison, with latency and training time reported for  $K = 10$  UEs.

- Parameters: Total number of trainable weights in the model.
- Memory (MB): Estimated memory footprint during inference, reflecting graphics processing unit (GPU) usage.
- FLOPs: Floating-point operations per forward pass, indicating computational complexity.
- Latency (ms): Average inference time, measuring real-time responsiveness.
- Training Time (s/epoch): Time per training epoch, capturing training efficiency.

ELU-CosFormer and CosFormer share the same architecture and parameter count, differing only in their activation functions—ELU and ReLU, respectively. Although ELU is computationally more intensive, ELU-CosFormer achieves slightly lower training time per epoch, due to smoother gradient flow that enables more efficient back-propagation and faster convergence. In contrast, ReLU's simplicity gives CosFormer a marginal advantage in inference latency, as ReLU operations are highly optimized

Table IV: Performance comparison of Transformer variants in terms of complexity and efficiency metrics.

Model	Parameters	Memory (MB)	FLOPs	Latency (ms)	Training Time (s/epoch)
ELU-CosFormer	103,378	0.39	1,056,820	3.42	858.27
CosFormer	103,378	0.39	1,056,820	3.40	915.82
Transformer	846,866	3.23	5,682,260	4.42	1447.69
Longformer	7,102,738	27.09	635,398,900	680.99	1866.63
Performer	103,378	0.39	1,041,460	4.40	1076.56

for GPU execution. Performer maintains a low parameter count and memory footprint comparable to CosFormer, but exhibits higher training and inference times due to the computational overhead of random feature projections and exponentiation in its kernel mapping [28], which are less GPU-efficient than CosFormer’s cosine reweighting.

The standard Transformer exhibits substantially higher FLOPs and memory requirements, owing to its quadratic attention mechanism and larger parameter count, resulting in increased latency and longer training time. Longformer shows the highest latency and training time overall, reflecting its significantly larger parameter count relative to the other models.

In summary, the results in Fig. 10 and Table IV indicate that the proposed ELU-CosFormer achieves the most balanced and scalable performance, validating its design for fairness-aware resource optimization.

### VII. Computational Complexity Analysis

When the number of users  $K$  increases, the per-sample computational complexity of our model is dominated by the linearized attention term  $\mathcal{O}(M \cdot d_{\text{mod}} \cdot K)$ , which scales linearly with  $K$ . This linear scaling represents a clear advantage compared to prior Transformer-based approaches [20], [23], where the complexity grows quadratically as  $\mathcal{O}(M \cdot d_{\text{mod}} \cdot K^2)$ , and iterative optimization methods [10], which scale as  $\mathcal{O}(T \cdot L \cdot K^2)$  with  $T$  iterations. It is also favorable compared to the optimal closed-form solution that require cubic scaling  $\mathcal{O}(K^3)$ , which quickly become prohibitive in dense networks.

For illustration, we benchmark the runtime on a CPU for  $K = 40$ , computing both AP-UE clusters and UL/DL powers using our predicted UC-CF scheme versus DCC (with closed-form solution for power computation). The proposed UC-CF model requires only 9.2ms, whereas DCC takes 31.6s. This orders-of-magnitude speedup, achieved through linearized attention, highlights the significant efficiency gain of our approach and makes it more suitable for large-scale deployments.

Beyond asymptotic complexity, several practical aspects reinforce the advantage of our model. The linear attention mechanism reduces memory usage compared to quadratic approaches, enabling scalability to larger user counts and deployment on resource-constrained edge devices. This efficiency also translates into lower energy consumption, aligning with sustainability goals in next-generation wireless networks. Moreover, the one-shot inference design avoids iterative overhead, ensuring real-time

responsiveness to dynamic user distributions and mobility. Importantly, the model maintains near-optimal SE despite its reduced complexity, confirming that efficiency does not compromise accuracy. Finally, linear attention benefits more from parallelization on graphics processing unit and tensor processing unit [38], [39], further widening the performance gap with quadratic and iterative methods.

### VIII. Conclusion

This paper proposed a scalable and flexible deep learning model for joint AP clustering and power allocation in UC CF mMIMO systems. The method follows a dynamic supervised learning paradigm in which optimal power labels are generated on the fly for the predicted AP clusters to train a CosFormer-based model that maps UE-AP spatial configurations to the corresponding resource allocation decisions. By relying primarily on spatial information and leveraging a customized attention mechanism, the proposed framework avoids pilot contamination, adapts seamlessly to varying user loads, and enables resource allocation decisions without requiring instantaneous channel information as input. This allows the joint clustering and power control to be decoupled from the data detection stage.

Numerical evaluations demonstrated that the proposed framework achieves near-optimal SE while reducing computational complexity and signaling overhead. In particular, while the complexity of the optimal solution scales as  $\mathcal{O}(K^3)$  with the number of UEs, the proposed model performs resource allocation through a single inference step and scales linearly with  $K$ . Furthermore, since the model relies only on spatial information during inference, it eliminates the need for exchanging instantaneous channels for resource optimization, thereby reducing signaling overhead. In addition, the clustering learned by the model limits the number of APs serving each UE to the most relevant ones, which further reduces coordination and signaling requirements between APs and the CPU.

Future research directions include investigating distributed learning strategies among APs or clusters to further reduce centralization requirements. Another promising direction is the integration of temporal information, enabling the model to capture user mobility, traffic variations, and time-dependent channel dynamics. Extending the architecture with temporal attention mechanisms may enable proactive resource allocation and enhance robustness in highly dynamic operating conditions. Additionally,

further validation could use ray-tracing datasets or real measurement campaigns.

## References

- [1] H. Q. Ngo, A. Ashikhmin, H. Yang, E. G. Larsson, and T. L. Marzetta, "Cell-free massive MIMO versus small cells," vol. 16, no. 3, pp. 1834–1850, 2017.
- [2] —, "Cell-free massive MIMO: Uniformly great service for everyone," in Proc. IEEE Intl. Work. Signal Process. Advances in Wireless Commun. (SPAWC), Stockholm, Sweden, 2015, pp. 201–205.
- [3] E. Nayebe, A. Ashikhmin, T. L. Marzetta, and H. Yang, "Cell-free massive MIMO systems," in Proc. Asilomar Conf. Signals, systems, and computers, Pacific Grove, CA, USA, 2015, pp. 695–699.
- [4] E. Björnson and L. Sanguinetti, "Making cell-free massive MIMO competitive with MMSE processing and centralized implementation," vol. 19, no. 1, pp. 77–90, 2019.
- [5] H. Q. Ngo, G. Interdonato, E. G. Larsson, G. Caire, and J. G. Andrews, "Ultradense cell-free massive MIMO for 6G: technical overview and open questions," vol. 112, no. 7, pp. 805–831, 2024.
- [6] Ö. T. Demir, E. Björnson, and L. Sanguinetti, "Foundations of user-centric cell-free massive MIMO," *Foundations and Trends® in Signal Processing*, vol. 14, no. 3-4, pp. 162–472, 2021.
- [7] S. Buzzi and C. D'Andrea, "Cell-free massive MIMO: User-centric approach," vol. 6, no. 6, pp. 706–709, 2017.
- [8] S. Buzzi, F. Linsalata, E. Moro, and G. Interdonato, "Why user-centric cell-free distributed MIMO systems will be the disruptive 6G technology," 2026, to appear.
- [9] E. Björnson and L. Sanguinetti, "A new look at cell-free massive MIMO: Making it practical with dynamic cooperation," in Proc. IEEE Intl. Symp. Personal, Indoor and Mobile Radio Commun. (PIMRC), Istanbul, Turkey, 2019.
- [10] M. Farooq, H. Q. Ngo, and L.-N. Tran, "Accelerated projected gradient method for the optimization of cell-free massive MIMO downlink," in Proc. IEEE Intl. Symp. Personal, Indoor and Mobile Radio Commun. (PIMRC), London, UK, 2020.
- [11] L. Miretti, R. L. G. Cavalcante, S. Stańczak, M. Schubert, R. Böhnke, and W. Xu, "Closed-form max-min power control for some cellular and cell-free massive MIMO networks," in Proc. IEEE Veh. Technol. Conf. (VTC), Helsinki, Finland, 2022.
- [12] E. Shi, J. Zhang, J. An, G. Zhang, Z. Liu, C. Yuen, and B. Ai, "Joint AP-UE association and precoding for SIM-aided cell-free massive MIMO systems," vol. 24, no. 6, pp. 5352–5367, 2025.
- [13] E. Björnson and E. Jorswieck, "Optimal resource allocation in coordinated multi-cell systems," *Foundations and Trends® in Communications and Information Theory*, vol. 9, no. 2-3, pp. 113–381, 2013.
- [14] H. A. Ammar, R. Adve, S. Shahbazpanahi, G. Boudreau, and K. V. Srinivas, "User-centric cell-free massive MIMO networks: A survey of opportunities, challenges and solutions," vol. 24, no. 1, pp. 611–652, 2021.
- [15] G. Di Gennaro, A. Buonanno, G. Romano, S. Buzzi, and F. A. Palmieri, "A deep learning approach for user-centric clustering in cell-free massive MIMO systems," in Proc. IEEE Intl. Work. Signal Process. Advances in Wireless Commun. (SPAWC), Lucca, Italy, 2024, pp. 661–665.
- [16] A. Liu and V. K. Lau, "Joint BS-user association, power allocation, and user-side interference cancellation in cell-free heterogeneous networks," vol. 65, no. 2, pp. 335–345, 2016.
- [17] H. A. Ammar, R. Adve, S. Shahbazpanahi, G. Boudreau, and K. V. Srinivas, "Downlink resource allocation in multiuser cell-free MIMO networks with user-centric clustering," vol. 21, no. 3, pp. 1482–1497, 2021.
- [18] Z. Liu, J. Zhang, Z. Liu, D. W. K. Ng, and B. Ai, "Joint cooperative clustering and power control for energy-efficient cell-free XL-MIMO with multi-agent reinforcement learning," vol. 72, no. 12, pp. 7772–7786, 2024.
- [19] A. Vaswani, N. Shazeer, N. Parmar, J. Uszkoreit, L. Jones, A. N. Gomez, Ł. Kaiser, and I. Polosukhin, "Attention is all you need," in Proc. Conf. Neural Inf. Process. Systems (NIPS), Long Beach, CA, USA, 2017.
- [20] A. K. Kocharlakota, S. A. Vorobyov, and R. W. Heath Jr, "Pilot contamination aware transformer for downlink power control in cell-free massive MIMO networks," vol. 25, pp. 9656–9671, 2026.
- [21] M. Dwarampudi and N. Reddy, "Effects of padding on LSTMs and CNNs," arXiv preprint arXiv:1903.07288, 2019.
- [22] F. Alrasheedi, X. Zhong, and P.-C. Huang, "Padding module: Learning the padding in deep neural networks," vol. 11, pp. 7348–7357, 2023.
- [23] I. Chafaa, G. Bacci, and L. Sanguinetti, "Transformer-based power optimization for max-min fairness in cell-free massive MIMO," vol. 14, no. 8, pp. 2316–2320, 2025.
- [24] S. Chakraborty, E. Björnson, and L. Sanguinetti, "Centralized and distributed power allocation for max-min fairness in cell-free massive MIMO," in Proc. Asilomar Conf. Signals, systems, and computers, Pacific Grove, CA, USA, 2019, pp. 576–580.
- [25] D. Kim, H. Jung, and I.-H. Lee, "A survey on deep learning-based resource allocation schemes," in Proc. Intl. Conf. Information and Commun. Technol. Convergence (ICTC), Jeju Island, South Korea, 2023.
- [26] Q. Mao, F. Hu, and Q. Hao, "Deep learning for intelligent wireless networks: A comprehensive survey," vol. 20, no. 4, pp. 2595–2621, 2018.
- [27] Z. Qin, W. Sun, H. Deng, D. Li, Y. Wei, B. Lv, J. Yan, L. Kong, and Y. Zhong, "cosFormer: Rethinking softmax in attention," arXiv preprint arXiv:2202.08791, 2022.
- [28] K. Choromanski, V. Likhoshesterov, D. Dohan, X. Song, A. Gane, T. Sarlos, P. Hawkins, J. Davis, A. Mohiuddin, L. Kaiser, D. Belanger, L. Colwell, and A. Weller, "Rethinking attention with performers," arXiv preprint arXiv:2009.14794, 2020.
- [29] S. Wang, B. Z. Li, M. Khabsa, H. Fang, and H. Ma, "Linformer: Self-attention with linear complexity," arXiv preprint arXiv:2006.04768, 2020.
- [30] I. Beltagy, M. E. Peters, and A. Cohan, "Longformer: The long-document transformer," arXiv preprint arXiv:2004.05150, 2020.
- [31] A. D. Rasamoelina, F. Adjailia, and P. Sinčák, "A review of activation function for artificial neural network," in Proc. IEEE World Symp. Applied Machine Intell. & Informatics (SAMI), Herlany, Slovakia, 2020.
- [32] C. Xue, P. Psimoulis, Q. Zhang, and X. Meng, "Analysis of the performance of closely spaced low-cost multi-gnss receivers," *Applied Geomatics*, vol. 13, no. 3, pp. 415–435, 2021.
- [33] V. Nasteski, "An overview of the supervised machine learning methods," *Horizons. b*, vol. 4, no. 51-62, p. 56, 2017.
- [34] H. Pham, Z. Dai, Q. Xie, and Q. V. Le, "Meta pseudo labels," in Proc. IEEE/CVF Conf. Computer Vision and Pattern Recognition, Nashville, TN, USA, 2021, pp. 11 557–11 568.
- [35] X. Wang, Z. Xu, D. Yang, L. Tam, H. Roth, and D. Xu, "Learning image labels on-the-fly for training robust classification models," arXiv preprint arXiv:2009.10325, 2020.
- [36] A. P. et al., "PyTorch: An imperative style, high-performance deep learning library," in Proc. Conf. Neural Inf. Process. Systems (NIPS), Vancouver, Canada, 2019.
- [37] P. Zhou, X. Xie, Z. Lin, and S. Yan, "Towards understanding convergence and generalization of AdamW," vol. 46d, no. 9, pp. 6486–6493, 2024.
- [38] S. Pal, V. Zhang, E. Ebrahimi, S. Migacz, A. Zulfqar, Y. Fu, D. Nellans, and P. Gupta, "Optimizing multi-GPU parallelization strategies for deep learning training," arXiv preprint arXiv:1907.13257, 2019.
- [39] N. P. Jouppi et al., "In-datacenter performance analysis of a tensor processing unit," in Proc. Annual Intl. Symp. Computer Architecture, Toronto, Canada, 2017, pp. 1–12.